

Handle Object Navigation as Weighted Traveling Repairman Problem

Ruimeng Liu, Xinhang Xu, Shenghai Yuan, *Member, IEEE* And Lihua Xie, *Fellow, IEEE*

Abstract—Zero-Shot Object Navigation (ZSON) requires agents to navigate to objects specified via open-ended natural language without predefined categories or prior environmental knowledge. While recent methods leverage foundation models or multi-modal maps, they often rely on 2D representations and greedy strategies or require additional training or modules with high computation load, limiting performance in complex environments and real applications. We propose WTRP-Searcher, a novel framework that formulates ZSON as a Weighted Traveling Repairman Problem (WTRP), minimizing the weighted waiting time of viewpoints. Using a Vision-Language Model (VLM), we score viewpoints based on object-description similarity, projected onto a 2D map with depth information. An open-vocabulary detector identifies targets, dynamically updating goals, while a 3D embedding feature map enhances spatial awareness and environmental recall. WTRP-Searcher outperforms existing methods, offering efficient global planning and improved performance in complex ZSON tasks. Code and more demos will be available on https://github.com/lrm20011/WTRP_Searcher.

I. INTRODUCTION

Zero-Shot Object Navigation (ZSON) is a challenging task in robotics and AI, where an agent is required to navigate to specified targets using open-ended natural language. Unlike conventional object navigation methods [1]–[4], ZSON operates without a predefined set of object categories or prior knowledge of the environment, making it more adaptable to real-world applications, as illustrated in Fig. 1.

Object navigation has received considerable research attention in recent years. Earlier works [5], [6] implicitly utilize the comprehension of the semantic environment through reinforcement or imitation learning but are limited to closed-set settings and certain environments. Recent training-free methods [7]–[9] leverage large language models (LLM) for planning by converting observations into language queries. However, this approach is inefficient and neglects complex 3D correspondence, leading to sub-optimal decisions. Many experiments in biology [10] and robotics [11], [12] have shown that spatial representation and memory are significant mechanisms in human navigation, and explicit maps improve performance and efficiency over end-to-end methods in various navigation tasks. More and more researchers are using prior map-based methods [13]. They build semantic

This work is supported by the National Research Foundation of Singapore under its Medium-Sized Center for Advanced Robotics Technology Innovation.

All authors are with the Centre for Advanced Robotics Technology Innovation (CARTIN), School of Electrical and Electronic Engineering, Nanyang Technological University, 50 Nanyang Avenue, Singapore 639798, {shyuan, elhxie}@ntu.edu.sg.



Fig. 1: Motivation of our work Zero-Shot Object Navigation in dealing with object-based navigation scenario without prior knowledge of the environment.

maps [14]–[17] for further inferring or decision making by close-set detector or open-vocabulary Vision-Language Model (VLM). Some works also combined this with a traditional frontier method, which marks the boundary of observed and unobserved areas for more efficient navigation [18], [19].

Despite these advancements, several challenges [20] remain in map-based and frontier-based approaches. Many methods [14], [16] employ top-down 2D feature maps, which struggle with overlapping objects and occluded environments (e.g., objects inside cabinets). Existing approaches [8], [19] often rely on greedy goal selection strategies, which choose the most promising viewpoint at each step but fail to account for long-term planning. This shortsighted decision-making can lead to inefficient search behaviors in complex environments.

To overcome these challenges, we propose WTRP-Searcher, a novel training-free navigation framework that formulates ZSON as a Weighted Traveling Repairman Problem (WTRP) to optimize search efficiency through global viewpoint selection. Our approach leverages a VLM to compute similarity scores between the environment and object descriptions, projecting them onto a 2D depth-enhanced map for improved spatial reasoning. Frontier-based viewpoint extraction assigns these similarity scores as weights in the WTRP optimization process, enabling more informed goal selection. Additionally, an open-vocabulary object detector dynamically refines candidate viewpoints and navigation targets based on detection confidence, while a 3D embedding feature map

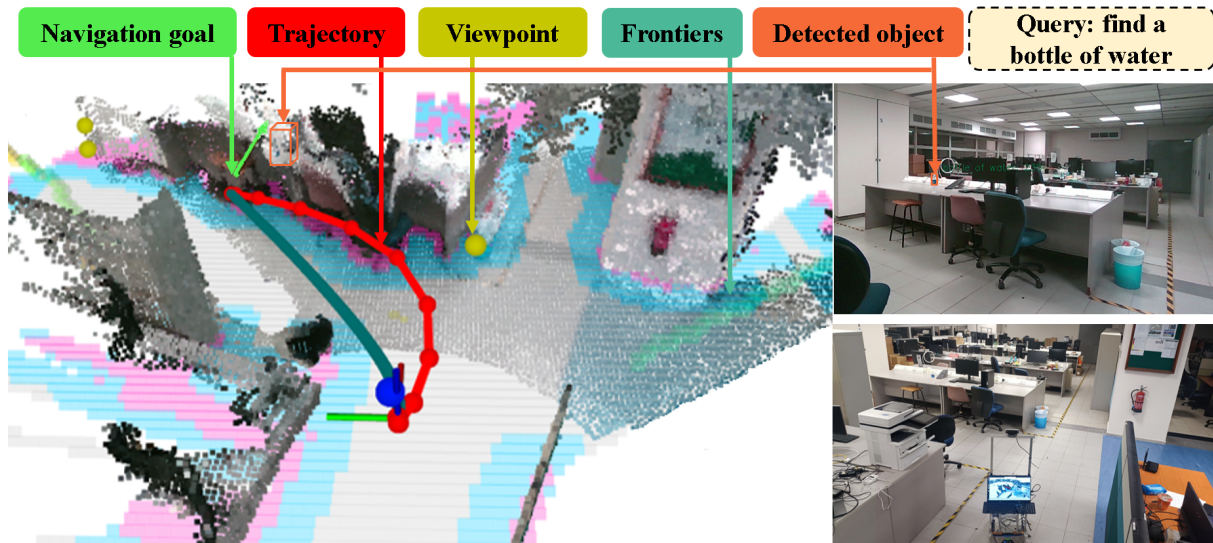


Fig. 2: Implementation of our approach in a real robot. The left image visualizes items that support the search framework. The right top image represents the detection result of a camera in the robot. The right bottom image is a third view.

continuously updates environment memory, enhancing object localization as the agent explores.

In general, the contributions of this work are as follows:

- We propose WTRP-Searcher, a training-free framework for Zero-Shot Object Navigation (ZSON) that integrates open-vocabulary detection, 3D feature mapping, and a Weighted Traveling Repairman Problem (WTRP) formulation for efficient global planning for object search.
- We introduce a global goal selection policy leveraging items and global associations, addressing the limitations of greedy strategies in prior work.
- We develop a real-time mapping system that builds multi-modal maps, enabling efficient object localization and environment memorization.
- We evaluate our method in simulated and real-world environments, showing superior performance over state-of-the-art approaches. We will open source our work for the benefit of society.

II. RELATED WORKS

A. Frontier-based Navigation

Frontier-based navigation is a widely used approach in exploration tasks, where frontiers mark the boundaries between explored and unexplored areas [21]. Classical methods often employ greedy strategies, selecting the nearest frontier at each step to maximize immediate exploration gains. More advanced strategies, such as next-best-view selection [22], evaluate candidate viewpoints based on information gain and path cost, selecting the one with the highest utility. To improve planning efficiency, recent works [23], [24] have reformulated frontier selection as a Traveling Salesman Problem (TSP), aiming to minimize the total travel cost across all viewpoints, which has demonstrated superior performance compared to traditional heuristic approaches [25]–[29].

Beyond general exploration, frontier-based strategies have been widely adopted in object search problems. Extensions of classical frameworks [30], [31] integrate unknown space exploration with object-centric surface inspection, enabling more target-aware navigation. Several works focus on leveraging frontier selection for object search optimization. For example, [18] introduces a learning-based policy that generates navigation goals based on semantic maps and frontiers, while [32] employs a simpler heuristic, iteratively selecting the closest frontier until an open-vocabulary detector confirms object detection. More recent approaches, such as VLF-M [19], combine visual-language similarity scoring with frontier selection, prioritizing viewpoints with the highest confidence to improve search efficiency.

This growing body of research highlights the effectiveness of frontier-based strategies in object search, yet many existing methods still suffer from greedy selection biases, lack of global planning, and reliance on 2D representations, which limits performance in complex, occluded, or long-horizon navigation tasks. Addressing these challenges remains a key direction for improving efficient and scalable object navigation.

B. Zero-Shot Object Navigation

ZSON requires an agent to navigate toward a specified target without prior training or exposure to the object or environment [33]. Traditional approaches can be broadly categorized into end-to-end learning methods and modular methods. End-to-end methods [34], [35] employ deep reinforcement learning (RL) or supervised learning to directly predict navigation actions from raw sensory inputs. Meanwhile, modular methods [6], [13] construct multi-modal maps that facilitate high-level decision-making and low-level motion planning, improving interpretability and structured reasoning. However,

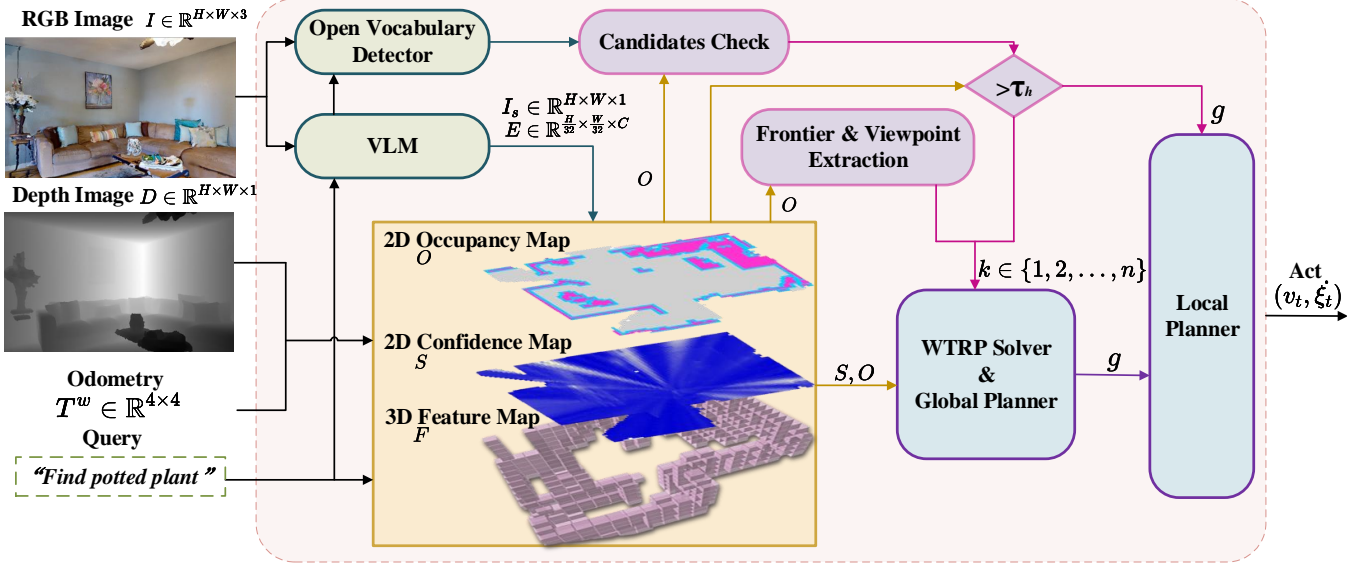


Fig. 3: Overview of our framework. Sub-modules are colored and classified according to their functionality. VLM and open-vocabulary detector perceive the environment and output features for mapping and planning; The mapping module constructs maps of three types from features, depth images, and poses; Modules in purple leverage detection results and multi-modal maps to generate candidate points for mid-term goals and potential navigation goals; All the candidate points are in overall planning by WTRP solver to get a global optimum route and the path to the first node would be sent to local planner to generate actions

both paradigms struggle with generalization, especially when encountering novel objects and unseen environments.

To address these limitations, recent works have explored foundation models [36]–[38] for object navigation, leveraging commonsense knowledge from large-scale internet datasets to improve adaptability. Some approaches [7]–[9] incorporate LLMs to generate text-based object queries or reason about object locations, enabling training-free exploration. Other methods [15], [39], [40] integrate VLMs as additional input to learning-based frameworks, enhancing scene understanding and target recognition. Additionally, recent works [16], [19] fuse VLMs with modular exploration methods, using semantic similarity scores to rank and prioritize navigation goals.

While these advances significantly improve zero-shot navigation capabilities, several challenges remain, including long-term spatial reasoning [41]–[50], scene understanding [51]–[56], efficient goal selection [57]–[59], and real-world deployment feasibility. Addressing these limitations is crucial for enabling robust, generalizable, and scalable ZSON solutions.

III. METHODOLOGY

In this section, we present the system architecture and the proposed methods in detail, outlining how our approach integrates global planning, semantic understanding, and multi-modal mapping to achieve efficient zero-shot object navigation.

A. Problem Formulation and System Overview

In a ZSON task, the agent must explore an unfamiliar environment to locate objects that match open-ended nat-

ural language descriptions. Unlike conventional navigation approaches that rely on predefined object categories or prior scene knowledge, zero-shot navigation requires the agent to interpret semantic queries dynamically and infer target locations in real time.

To achieve this, the agent receives an RGB image stream, an aligned depth image, and pose information as inputs. These sensory data are used to construct a spatial representation of the environment, allowing the agent to reason about potential object locations. Based on this representation, the agent plans a trajectory or generates a sequence of actions to navigate efficiently toward the target object. The overall architecture of our framework is illustrated in Figure 3, detailing the integration of multi-modal perception, mapping, and goal selection to enable efficient object search.

B. Map Construction

Given an RGB image $I \in \mathbb{R}^{H \times W \times 3}$, we extract features and project points into world space using an aligned depth image $D \in \mathbb{R}^{H \times W \times 1}$, camera parameters, and the pose transformation matrix $T^w \in \mathbb{R}^{4 \times 4}$. This process constructs three complementary maps: a 2D occupancy grid map O for navigation and exploration, a 2D semantic confidence map S for goal selection, and a 3D feature map F for object matching.

1) *Occupancy Grid Map*: Each cell in the 2D occupancy grid map holds a probability value and an inflation count, indicating whether it is occupied, free, unknown, or influenced by nearby occupied grids. The map is generated by projecting depth points onto a 2D grid, applying raycasting to classify grid cells as hits or misses, and updating their state using a Bayesian approach. After each update, surrounding grids are

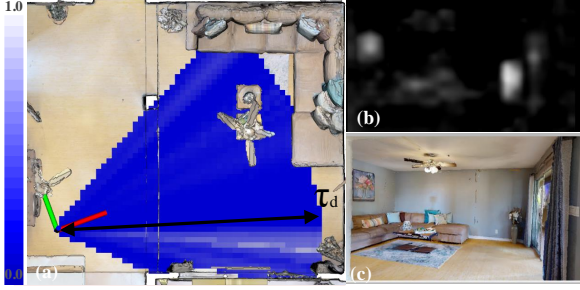


Fig. 4: Construct a temporal confidence map. (a) is the construction result. (b) is a pixel-wise confidence image generated from (c) by VLM. The mapping is limited in τ_d while points outside the region would also slightly contribute to the updating to enhance semantic guidance for navigation.

adjusted to reflect obstacle inflation, improving navigation safety.

2) *Semantic Similarity Map*: To integrate semantic awareness into navigation, we construct a 2D semantic similarity map using vision-language embeddings. Given an RGB image $I \in \mathbb{R}^{H \times W \times 3}$, we use a CLIP-based feature extractor [60], [61] to obtain patch-level embeddings $E \in \mathbb{R}^{H/32 \times W/32 \times C}$, where C denotes the embedding dimension. The cosine similarity between target descriptions and image patches is computed and upsampled to form a full-image similarity map $I_s \in \mathbb{R}^{H \times W \times 1}$.

These 2D similarity values are then projected into 3D world space using the aligned depth image $D \in \mathbb{R}^{H \times W \times 1}$ and the pose transformation matrix $T^w \in \mathbb{R}^{4 \times 4}$. To enhance robustness, the top 20% similarity values are averaged at each spatial location, denoted as S_p^t . The covariance of the similarity value at grid cell p is then computed as:

$$\sigma_p^{2t} = \frac{\alpha_c * (d_{p,p_0})^2}{n_p}, \quad (1)$$

where n_p is the number of points in the 2D grid, d_{p,p_0} represents the distance of the grid to the sensor origin p_0 , and α_c is a scaling factor.

To maintain consistency over time, we employ a Kalman filter to update the similarity value S_p in grid p using the current observation S_p^t :

$$K = \frac{\sigma_p^{2t}}{\sigma_p^{2-} + \sigma_p^{2t}}, \quad (2)$$

$$S_p = S_p^t + K(S_p^- - S_p^t), \quad (3)$$

$$\sigma_p^2 = (1 - K)\sigma_p^{2t}. \quad (4)$$

For multi-object navigation, a separate similarity map is maintained for each object category, following the same projection and fusion process. To evaluate viewpoints in unexplored free space, similarity values for unobserved grids p' are estimated by raycasting from observed grids p :

$$S_{p'}^t = S_p^t - \gamma d_{p,p'}, \quad (5)$$

$$\sigma_{p'}^{2t} = \beta \sigma_p^{2t}, \quad (6)$$

where γ and β control similarity decay over distance. To mitigate depth sensor noise, points exceeding the threshold τ_d are removed, while virtual points at distance τ_d along the ray from the sensor are introduced. The similarity of these virtual points follows Equation 1. Figure 4 illustrates the process of constructing a temporal confidence map S^t from an observation.

Algorithm 1: Procedure to visit a cuboid

Input: $P, E \in \mathbb{R}^{H/32 \times W/32 \times C}$

Output: F^t

```

1: for  $h = 0$  to  $H$  do
2:   for  $w = 0$  to  $W$  do
3:     if !NeedDownsample( $h, w$ ) then
4:        $id \leftarrow PosToIndex(P_{h,w})$ 
5:        $(p_i^E, \omega_i), i \in 0, 1, 2, 3 \leftarrow GetRelatedPixels(h, w)$ 
6:        $L \leftarrow M_f(id)$ 
7:       if  $L$  Occurs then
8:         for  $(p_i^E, \omega_i), i \in 0, 1, 2, 3$  do
9:           if  $L(p_i^E)$  Occurs then
10:             $L(p_i^E)+ = \omega_i$ 
11:          else
12:             $L.Insert(p_i^E, \omega_i)$ 
13:          end if
14:        end for
15:      else
16:         $M_f.Insert(id, (p_i^E, \omega_i), i \in 0, 1, 2, 3)$ 
17:      end if
18:    end if
19:  end for
20: end for
21: for  $m \in M_f$  do
22:    $v = Zero()$ 
23:   for  $(p, \omega) \in m.value$  do
24:      $v+ = \omega * E_p$ 
25:   end for
26:    $v.Normalization()$ 
27:    $F^t.Insert(m.key, v)$ 
28: end for
29: return  $F^t$ 

```

3) *3D Feature Map*: Following the procedure described in subsection III-B2, at each time step t , we project feature embeddings into 3D space using aligned depth images and pose information. The average embedding F_p^t is computed for all embeddings mapped to the same 3D grid cell p . To maintain temporal consistency, we apply a Kalman filter to fuse F_p^t with the previous feature map F_p , with the covariance and update equations following Equation 1 and Equation 2, respectively. For efficient storage and traversal, we employ a modified octree structure [62], which exclusively stores occupied grids with embeddings. Additionally, grids corresponding to the floor and ceiling are systematically eliminated based on height thresholds, further optimizing the representation.

Since the vision-language model (VLM) we employ pro-

duces patch-level features $E \in \mathbb{R}^{H/32 \times W/32 \times C}$, bilinear interpolation is typically used to obtain image-level features $E' \in \mathbb{R}^{H \times W \times C}$. However, performing interpolation during the fusion process introduces significant computational and storage overhead. To mitigate this, we omit the interpolation step in the feature fusion process, as demonstrated in algorithm 1.

Instead of directly distributing feature embeddings when projecting aligned depth points from $D \in \mathbb{R}^{H \times W \times 1}$ to 3D grids, we propagate the percentage of pixels in $E \in \mathbb{R}^{H/32 \times W/32 \times C}$ that contribute to corresponding pixels in D . This strategy significantly reduces the number of high-dimensional embeddings processed during fusion.

In algorithm 1, $P_{h,w}$ denotes the 3D world coordinates of a pixel $(h, w) \in D$. The function $M_f(id, L)$ maintains a mapping of keys id to value lists L , where $M_f(id) = L$. The list $L(p^E, \omega)$ stores pairs of pixels from $E \in \mathbb{R}^{H/32 \times W/32 \times C}$ and their corresponding weights ω , which are used to compute the weighted sum of feature embeddings in each 3D grid cell, where $L(p^E) = \omega$.

C. Mid-term Goal Choosing Policy

Recent advancements in exploration tasks have formulated the problem of visiting all viewpoints as a Traveling Salesman Problem (TSP), aiming to minimize the length of the global tour. However, directly applying this formulation to object search tasks may not be optimal, as the agent stops once it finds a target—meaning that, in most cases, not all viewpoints are visited. Additionally, from a behavioral perspective, viewpoints with higher semantic similarity to the target should be prioritized over purely minimizing the travel distance. A global tour optimization that neglects semantic relevance may result in suboptimal search efficiency.

Following [63], we define the Weighted Traveling Repairman Problem (WTRP) as follows:

Given a set of points $k \in \{0, 1, \dots, n\}$ with associated weights W_k , a cost matrix M_{k_r, k_s} representing the time cost between any two points k_r and k_s , and a start point $0 \in \{0, 1, \dots, n\}$, the goal is to find a permutation $\pi_0 = 0, \pi_1, \dots, \pi_n$ that minimizes:

$$\min_{\pi} \sum_{i=1}^n w_{\pi_i} \sum_{j=1}^i M_{\pi_{j-1}, \pi_j}, \quad (7)$$

where π_j denotes the j -th node to be visited, π_0 is the agent's current position, and W_{π_j} is the weight of the node, computed as:

W_{π_j} denotes the weight of nodes and can be gained from:

$$W_{\pi_j} = \phi(S_{p_{\pi_j}}), \quad (8)$$

$$\phi(x) = \alpha_s e^{\mu x + \nu}, \quad (9)$$

where $\phi(x)$ is a mapping function designed to amplify the differences in node weights. The parameters α_s , μ , and ν are scaling factors.

Here, p_k represents the position of a viewpoint or the agent in the map, and $S_{p_{\pi_j}}$ is the similarity of the node, which can be retrieved from the 2D similarity map based on its location.

Additionally, each viewpoint $k \in \{1, 2, \dots, n\}$ has a yaw angle ξ_k that describes its orientation.

Inspired by [23], [64], we incorporate both the distance between nodes and the agent's motion state—where v_0 and ξ_0 denote the agent's current velocity and orientation, while v_{max} and ξ_{max} represent its maximum linear and angular velocities. The cost matrix is then defined as:

$$t(k_r, k_s) = \max\left\{\frac{d_{p_{k_r}, p_{k_s}}}{v_{max}}, \frac{|\xi_{k_r} - \xi_{k_s}|}{\xi_{max}}\right\}, \quad (10)$$

$$c_c(k) = \cos^{-1} \frac{(p_k - p_0) \cdot v_0}{\|p_k - p_0\| \|v_0\|}, \quad (11)$$

$$c_s(k) = \frac{h_k}{h_{max}}, \quad (12)$$

$$M_{0,k} = t(0, k) + w_c \cdot c_c(k) + w_f \cdot c_s(k), \quad (13)$$

$$k \in 1, 2, \dots, n,$$

$$M_{k_r, k_s} = M_{k_s, k_r} = t(k_r, k_s), \quad (14)$$

$$k_r, k_s \in 1, 2, \dots, n,$$

$$M_{k,0} = 0, \quad (15)$$

where $t(k_r, k_s)$ denotes the travel time between nodes k_r and k_s , while $c_c(k)$ ensures motion consistency. The term $c_s(k)$ is introduced to encourage the agent to first explore small, enclosed unexplored areas, which often result from incomplete observations and could otherwise cause inefficient back-and-forth maneuvers.

To compute h_k , a ray is cast from the viewpoint toward the cluster center of its frontiers. If the ray intersects observed grids within the distance threshold h_{max} , h_k is set as the distance from the hit grid to the cluster center. Otherwise, h_k defaults to h_{max} .

We solve the WTRP using the LKH solver [65]. The first viewpoint in the computed tour serves as the next navigation goal. If the agent reaches a mid-term goal or the execution time exceeds the replan threshold τ_r , we recompute the global tour to accommodate newly added candidate viewpoints dynamically.

D. Candidate Generation Policy

Candidate points for the next mid-term goal are selected from frontier cluster viewpoints, feature map matching results, and detections from an open-vocabulary object detector.

In an unknown environment, frontiers are extracted from free-space grid cells adjacent to unknown regions. Viewpoints are then generated by clustering these frontiers in previously visited free space, ensuring an optimal vantage point for exploration.

During navigation, an open-vocabulary detector continuously searches for target categories. We utilize YOLO-World [66] for real-time object detection. If the confidence score of a detected object exceeds the threshold τ_h , its corresponding viewpoint is immediately set as the next navigation goal g . For objects with confidence scores between τ_l and τ_h , the viewpoint is added as a candidate point for consideration

TABLE I: Comparison with baselines in single-object navigation.

| Method | Training-free | Foundation Model | HM3D | |
|--------------|---------------|------------------|-------------|-------------|
| | | | SR↑(%) | SPL↑(%) |
| ZSON [39] | × | CLIP | 25.5 | 12.6 |
| Voronav [69] | ✓ | GPT-3.5 | 42.0 | 26.0 |
| ESC [8] | ✓ | GLIP, GPT-3.5 | 39.2 | 22.3 |
| VLFM [19] | × | BLIP2 | 52.5 | 30.4 |
| Ours | ✓ | CLIP | 59.2 | 38.9 |

in the WTRP solver. Since high-confidence detections can sometimes be false positives due to specific viewing angles or distances, detected targets are re-evaluated during navigation. If the confidence score drops below τ_h for a sustained period, the target is removed from the candidate list.

As the agent navigates, a 3D feature map is built and continuously updated. This map enhances the system’s environment memorization capability, improving target localization. Given a language-based query, we compute the similarity between the description and stored embeddings in each 3D grid. Similar to object detections, viewpoints corresponding to high-confidence grid cells are directly treated as navigation goals g , while those with slightly lower confidence are incorporated into the WTRP solver for optimized selection.

E. Local Planner

Once a navigation goal g is selected, a suitable path is generated based on the distance from the agent’s current position. If the target is farther away, waypoints are computed using the A* algorithm, whereas single-point goals are directly sent to the local planner. For trajectory optimization, we adapt the local planner from [67], leveraging MINCO [68] to ensure smooth motion planning. The final linear and angular velocity commands (v_t, ξ_t) for the chassis are generated by a low-level controller. The local planner is capable of handling dynamic obstacles and producing smooth, collision-free trajectories, thereby enhancing the system’s robustness and overall performance.

IV. EXPERIMENTS

In this section, we evaluate our method using the Habitat simulator on the HM3D dataset [70] by comparing it with baseline methods in both single-object and multi-object navigation tasks. We further validate our approach through real-world experiments.

A. Single Object Navigation

This task requires the agent to locate an object belonging to the target category in an unknown environment. We evaluate our method using the validation split of the HM3D dataset, which consists of 2000 single-object navigation episodes across 20 scenes and 6 object categories.

Evaluation Metrics: We use standard evaluation metrics, including Success Rate (SR) in % and Success weighted by Path Length (SPL) in %. SR measures the proportion of successful episodes, while SPL accounts for both success

TABLE II: Multi-object navigation evaluation

| Method | Type | HM3D | | | |
|-------------|--------------|-------------|-------------|-------------|-------------|
| | | SR↑(%) | SPL↑(%) | PR↑(%) | PPL↑(%) |
| TSP Exp | Simultaneous | 29.3 | 12.1 | 49.3 | 17.8 |
| W/o CGP | | 35.1 | 15.4 | 57.5 | 19.4 |
| W/o WTRP | | 48.7 | 16.1 | 66.2 | 21.2 |
| Ours | | 53.4 | 23.1 | 69.2 | 29.3 |
| OneMap [16] | Sequential | 54.2 | 27.8 | 65.5 | 32.7 |
| Ours | | 54.7 | 32.3 | 66.1 | 35.4 |

and path efficiency, computed as the ratio of the optimal path length to the actual path length, weighted by a binary success indicator.

Baseline Selection: We compare our approach against the current state-of-the-art (SOTA) methods in zero-shot object navigation, including ZSON [39], VoroNav [69], ESC [8], and VLFM [19]. ZSON is a learning-based method that incorporates vision-language model (VLM) embeddings as input. VoroNav constructs a Voronoi graph from a semantic map, enabling a large language model (LLM) to reason about waypoints. ESC and VLFM both employ frontiers for navigation: ESC utilizes a VLM for scene understanding and an LLM for goal selection, while VLFM ranks frontiers based on VLM similarity scores, selecting the highest-scoring frontier as the next waypoint.

Results Discussion: The results of our comparison are presented in Table I. Our method achieves superior performance over all zero-shot SOTA baselines in both SR and SPL. Specifically, we obtain an SR of 0.592 and an SPL of 0.389, representing a 12.7% improvement in SR and a 27.9% improvement in SPL compared to VLFM.

We attribute our higher SR to our candidate selection policy, where rechecking detected objects reduces the false positive rate, leading to more reliable target identification. Our significant SPL improvement indicates that formulating the route planning problem as a WTRP leads to more efficient trajectories compared to frontier-based approaches that greedily select the highest-scoring frontier. Additionally, the use of patch-level CLIP embeddings enables a more detailed and structured understanding of the environment than image-level visual-language models, allowing the constructed value map to guide exploration more effectively.

B. Multi-Object Navigation

For multi-object navigation tasks, we design two types of experiments. In the first setting, the agent is given a list of target categories at the beginning and is required to find at least one object for each category. In the second setting, the agent receives the target categories sequentially, where a new target is assigned only after the current one is found. We evaluate our approach on the benchmark from [16], which consists of 236 episodes in 20 scenes across six categories. Each episode includes three target categories, and the agent has no prior knowledge of the scene.

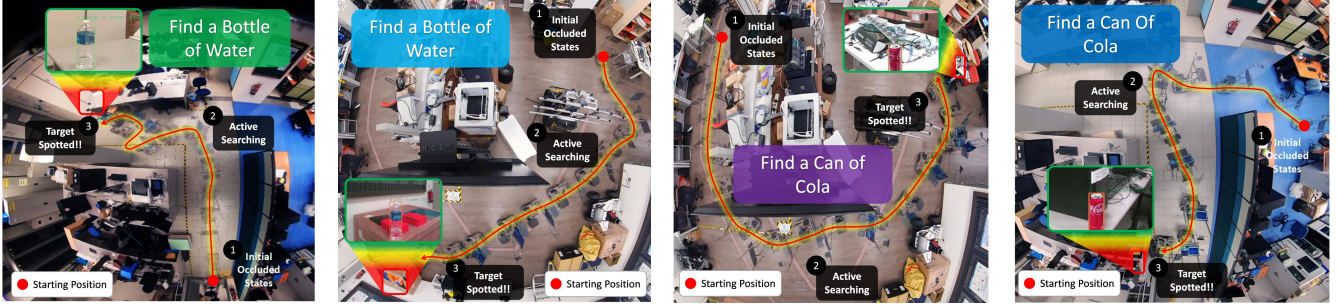


Fig. 5: The process of visual language navigation in two real office scenes over two categories.

Evaluation Metrics: In addition to the metrics defined in subsection IV-A, we introduce additional metrics for multi-object navigation: Progress Rate (PR) in %, which measures the rate at which the agent makes progress toward finding all target objects, and Progress Weighted by Path Length (PPL) in %, defined as:

$$\text{PPL} = \frac{1}{N} \sum_{i=1}^N r_i \frac{l_i}{\max(p_i, l_i)},$$

where N is the number of episodes, l_i is the optimal path length for episode i , and r_i and p_i represent the PR and the actual total path length of episode i , respectively.

Baseline Selection: We compare our method with OneMap [16], which is designed for sequential multi-object navigation and constructs a 2D feature map storing VLM embeddings. As no recent open-source approaches are available for simultaneous multi-object navigation, we conduct an ablation study to evaluate the impact of our framework’s key components. Specifically, it includes replacing the WTRP solver with a greedy strategy (“W/o WTRP”), eliminating candidates for global planner from detection and match results (“W/o CGP”), and adopting a TSP-based exploration framework that explores and detects the environment separately (“TSP Exp”), as shown in Table II.

Results Discussion: The results in Table II demonstrate the effectiveness of our core technical components. The superior performance over the other methods in simultaneous planning underscores the advantage of our WTRP formulation in facilitating global, long-term planning. Compared to OneMap’s sequential planning, WTRP-Searcher exhibits improvements in SPL (0.323 vs. 0.278) and PPL (0.354 vs. 0.327), highlighting the synergy between global WTRP optimization and the 3D feature map. The feature map’s capability to store and match environmental embeddings enables the agent to efficiently revisit high-similarity regions, reducing redundant exploration.

C. Real World Experiments

We deploy our method on a differential-drive robot equipped with a RealSense D455 depth camera, which provides RGB-D images. For odometry estimation, we utilize RTAB-Map [71], leveraging both RGB-D images and IMU data from the D455 camera. The entire system is implemented on a Jetson Orin NX 16GB platform.

TABLE III: Time consumption of sub-modules on ORIN. In a Desktop PC, the performance can be doubled. We show the worst-case performance. An asterisk (*) indicates that the sub-module may also be triggered by external signals.

| Task | Time consumption (s) | Desired interval (s) |
|--------------------------|----------------------|----------------------|
| VLM | 0.011 | 0.125 |
| Open-vocabulary detector | 0.079 | 0.125 |
| 2D grid map | 0.108 | 0.125 |
| 2D confidence map | 0.129 | 0.125 |
| 3D feature map | 0.589 | 0.250 |
| WTRP solver | 0.010 | 5.000* |
| Trajectory optimization | 0.005 | 0.500* |

The time consumption of each sub-module per iteration, along with its desired updating interval, is summarized in Table III. These results demonstrate the efficiency of our system, highlighting its feasibility for real-world robotic deployment. Although 3D feature map looks a bit heavy for the embedded device, the module serves to match language with the environment when receiving queries, and the latency in construction does not influence search. Figure 5 illustrates top-down trajectories across four distinct scenarios, demonstrating the agent’s ability to navigate around objects effectively. Further implementation details can be found in the accompanying video.

V. CONCLUSION

In this work, we introduced WTRP-Searcher, a novel framework for Zero-Shot Object Navigation (ZSON) that formulates the task as a Weighted Traveling Repairman Problem (WTRP). Our approach integrates frontier-based exploration, open-vocabulary object detection, and 3D feature map matching to dynamically select candidate viewpoints and navigation goals. By combining global planning via WTRP with a robust local planner, WTRP-Searcher enables smooth, efficient, and obstacle-aware navigation. Experimental results demonstrate that our method outperforms state-of-the-art approaches in efficiency, accuracy, and adaptability, validating its effectiveness in both simulated and real-world environments.

These findings underscore the importance of integrating spatial reasoning, semantic understanding, and global optimization to enhance ZSON capabilities in robotic applications. Building on this foundation, future research will explore lifelong learning for continuous adaptation and domain

adaptation for effective sim-to-real transfer, further improving the robustness and generalization of robotic navigation.

REFERENCES

- [1] K. Cao, M. Cao, S. Yuan, and L. Xie, "Direct: A differential dynamic programming based framework for trajectory generation," *IEEE Robotics and Automation Letters*, vol. 7, no. 2, pp. 2439–2446, 2022.
- [2] T. Hu, S. Yuan, R. Bai, and X. Xu, "Swept volume-aware trajectory planning and mpc tracking for multi-axle swerve-drive amrs," in *2025 IEEE International Conference on Robotics and Automation (ICRA)*, 2025.
- [3] R. Bai, S. Yuan, K. Li, H. Guo, W.-Y. Yau, and L. Xie, "Realm: Real-time line-of-sight maintenance in multi-robot navigation with unknown obstacles," in *IEEE International Conference on Robotics and Automation (ICRA)*, 2025.
- [4] K. Wu, M. A. Esfahani, S. Yuan, and H. Wang, "Depth-based obstacle avoidance through deep reinforcement learning," in *Proceedings of the 5th International Conference on Mechatronics and Robotics Engineering*, 2019, pp. 102–106.
- [5] E. Wijmans, A. Kadian, A. Morcos, S. Lee, I. Essa, D. Parikh, M. Savva, and D. Batra, "Dd-ppo: Learning near-perfect pointgoal navigators from 2.5 billion frames," in *International Conference on Learning Representations (ICLR)*, 2020.
- [6] M. Chang, A. Gupta, and S. Gupta, "Semantic visual navigation by watching youtube videos," *Advances in Neural Information Processing Systems*, vol. 33, pp. 4283–4294, 2020.
- [7] B. Yu, H. Kasaei, and M. Cao, "L3mvt: Leveraging large language models for visual target navigation," in *Proc. IEEE/RSJ International Conference on Intelligent Robots and Systems (IROS)*, 2023.
- [8] K. Zhou, K. Zheng, C. Pryor, Y. Shen, H. Jin, L. Getoor, and X. E. Wang, "Esc: Exploration with soft commonsense constraints for zero-shot object navigation," in *International Conference on Machine Learning*. PMLR, 2023, pp. 42829–42842.
- [9] V. S. Dorbala, J. F. Mullen, and D. Manocha, "Can an embodied agent find your 'cat-shaped mug'? llm-based zero-shot object navigation," *IEEE Robotics and Automation Letters*, 2024.
- [10] R. G. Golledge, *Wayfinding behavior: Cognitive mapping and other spatial processes*. JHU press, 1999.
- [11] D. S. Chaplot, R. Salakhutdinov, A. Gupta, and S. Gupta, "Neural topological slam for visual navigation," in *Proceedings of the IEEE/CVF conference on computer vision and pattern recognition*, 2020.
- [12] D. S. Chaplot, D. Gandhi, S. Gupta, A. Gupta, and R. Salakhutdinov, "Learning to explore using active neural slam," in *International Conference on Learning Representations (ICLR)*, 2020.
- [13] D. S. Chaplot, D. P. Gandhi, A. Gupta, and R. R. Salakhutdinov, "Object goal navigation using goal-oriented semantic exploration," *Advances in Neural Information Processing Systems*, 2020.
- [14] C. Huang, O. Mees, A. Zeng, and W. Burgard, "Visual language maps for robot navigation," in *2023 IEEE International Conference on Robotics and Automation (ICRA)*. IEEE, 2023, pp. 10608–10615.
- [15] M. Wei, T. Wang, Y. Chen, H. Wang, J. Pang, and X. Liu, "Ovexp: Open vocabulary exploration for object-oriented navigation," *arXiv preprint arXiv:2407.09016*, 2024.
- [16] F. Lukas Busch, T. Homberger, J. Ortega-Peimbert, Q. Yang, and O. Andersson, "One map to find them all: Real-time open-vocabulary mapping for zero-shot multi-object navigation," *arXiv e-prints*, pp. arXiv-2409, 2024.
- [17] B. Yu, Y. Liu, L. Han, H. Kasaei, T. Li, and M. Cao, "VIn-game: Vision-language equilibrium search for zero-shot semantic navigation," *arXiv preprint arXiv:2411.11609*, 2024.
- [18] B. Yu, H. Kasaei, and M. Cao, "Frontier semantic exploration for visual target navigation," in *Proc. IEEE International Conference on Robotics and Automation (ICRA)*, 2023.
- [19] N. Yokoyama, S. Ha, D. Batra, J. Wang, and B. Bucher, "Vlfm: Vision-language frontier maps for zero-shot semantic navigation," in *2024 IEEE International Conference on Robotics and Automation (ICRA)*. IEEE, 2024, pp. 42–48.
- [20] S. Yuan, H. Wang, and L. Xie, "Survey on localization systems and algorithms for unmanned systems," *Unmanned Systems*, vol. 9, no. 02, pp. 129–163, 2021.
- [21] B. Yamauchi, "A frontier-based approach for autonomous exploration," in *Proceedings 1997 IEEE International Symposium on Computational Intelligence in Robotics and Automation CIRA'97. Towards New Computational Principles for Robotics and Automation*. IEEE, 1997, pp. 146–151.
- [22] A. Bircher, M. Kamel, K. Alexis, H. Oleynikova, and R. Siegwart, "Receding horizon path planning for 3d exploration and surface inspection," *Autonomous Robots*, vol. 42, pp. 291–306, 2018.
- [23] B. Zhou, Y. Zhang, X. Chen, and S. Shen, "Fuel: Fast uav exploration using incremental frontier structure and hierarchical planning," *IEEE Robotics and Automation Letters*, vol. 6, no. 2, pp. 779–786, 2021.
- [24] Y. Zhao, L. Yan, H. Xie, J. Dai, and P. Wei, "Autonomous exploration method for fast unknown environment mapping by using uav equipped with limited fov sensor," *IEEE Transactions on Industrial Electronics*, vol. 71, no. 5, pp. 4933–4943, 2023.
- [25] Y. Lyu, S. Yuan, and L. Xie, "Structure priors aided visual-inertial navigation in building inspection tasks with auxiliary line features," *IEEE Transactions on Aerospace and Electronic Systems*, vol. 58, no. 4, pp. 3037–3048, 2022.
- [26] K. Wu, H. Wang, M. A. Esfahani, and S. Yuan, "Bnd*-ddqn: Learn to steer autonomously through deep reinforcement learning," *IEEE Transactions on Cognitive and Developmental Systems*, vol. 13, no. 2, pp. 249–261, 2019.
- [27] Y. Lyu, T.-M. Nguyen, L. Liu, M. Cao, S. Yuan, T. H. Nguyen, and L. Xie, "Spins: A structure priors aided inertial navigation system," *Journal of Field Robotics*, vol. 40, no. 4, pp. 879–900, 2023.
- [28] K. Wu, H. Wang, M. A. Esfahani, and S. Yuan, "Learn to navigate autonomously through deep reinforcement learning," *IEEE Transactions on Industrial Electronics*, vol. 69, no. 5, pp. 5342–5352, 2021.
- [29] M. J. Er, S. Yuan, and N. Wang, "Development control and navigation of octocopter," in *2013 10th IEEE International Conference on Control and Automation (ICCA)*. IEEE, 2013, pp. 1639–1643.
- [30] S. Papatheodorou, N. Funk, D. Tzoumanikas, C. Choi, B. Xu, and S. Leutenegger, "Finding things in the unknown: Semantic object-centric exploration with an mav," in *Proc. IEEE International Conference on Robotics and Automation (ICRA)*, 2023.
- [31] Y. Luo, Z. Zhuang, N. Pan, C. Feng, S. Shen, F. Gao, H. Cheng, and B. Zhou, "Star-searcher: A complete and efficient aerial system for autonomous target search in complex unknown environments," *IEEE Robotics and Automation Letters*, 2024.
- [32] S. Y. Gadre, M. Wortsman, G. Ilharco, L. Schmidt, and S. Song, "Cows on pasture: Baselines and benchmarks for language-driven zero-shot object navigation," in *Proceedings of the IEEE/CVF Conference on Computer Vision and Pattern Recognition*, 2023, pp. 23171–23181.
- [33] L. Chen, C. Liang, S. Yuan, M. Cao, and L. Xie, "Relative localizability and localization for multi-robot systems," *IEEE Transactions on Robotics*, 2025.
- [34] P. Mirowski, R. Pascanu, F. Viola, H. Soyer, A. Ballard, A. Banino, M. Denil, R. Goroshin, L. Sifre, K. Kavukcuoglu, D. Kumaran, and R. Hadsell, "Learning to navigate in complex environments," in *International Conference on Learning Representations (ICLR)*, 2017.
- [35] R. Ramrakhya, E. Undersander, D. Batra, and A. Das, "Habitat-web: Learning embodied object-search strategies from human demonstrations at scale," in *Proc. of the IEEE/CVF conference on computer vision and pattern recognition*, 2022.
- [36] Y. Lai, S. Yuan, Y. Nassar, M. Fan, A. Gopal, A. Yorita, N. Kubota, and M. Rättsch, "Nmm-hri: Natural multi-modal human-robot interaction with voice and deictic posture via large language model," *IEEE Robotics and Automation Magazine (RAM)*, 2025.
- [37] Y. Lai, S. Yuan, Y. Nassar, M. Fan, T. Weber, and M. Rättsch, "Nvp-hri: Zero shot natural voice and posture-based human-robot interaction via large language model," *Expert Systems with Applications*, vol. 268, p. 126360, 2025.
- [38] Z. Qi, S. Yuan, F. Liu, H. Cao, T. Deng, J. Yang, and L. Xie, "Air-embodied: An efficient active 3dgs-based interaction and reconstruction framework with embodied large language model," in *arXiv preprint arXiv:2409.16019*, 2024.
- [39] A. Majumdar, G. Aggarwal, B. Devnani, J. Hoffman, and D. Batra, "Zson: Zero-shot object-goal navigation using multimodal goal embeddings," *Advances in Neural Information Processing Systems*, 2022.
- [40] Q. Zhao, L. Zhang, B. He, H. Qiao, and Z. Liu, "Zero-shot object goal visual navigation," in *2023 IEEE International Conference on Robotics and Automation (ICRA)*. IEEE, 2023, pp. 2025–2031.

- [41] X. Ji, S. Yuan, J. Li, P. Yin, H. Cao, and L. Xie, "Sgba: Semantic gaussian mixture model-based lidar bundle adjustment," *IEEE Robotics and Automation Letters*, vol. 9, no. 12, pp. 10922–10929, 2024.
- [42] Z. Chen, Y. Xu, S. Yuan, and L. Xie, "ig-lid: An incremental gicp-based tightly-coupled lidar-inertial odometry," *IEEE Robotics and Automation Letters*, vol. 9, no. 2, pp. 1883–1890, 2024.
- [43] X. Ji, S. Yuan, P. Yin, and L. Xie, "Lio-gvm: an accurate, tightly-coupled lidar-inertial odometry with gaussian voxel map," *IEEE Robotics and Automation Letters*, vol. 9, no. 3, pp. 2200–2207, 2024.
- [44] J. Li, T.-M. Nguyen, S. Yuan, and L. Xie, "Pss-ba: Lidar bundle adjustment with progressive spatial smoothing," in *2024 IEEE/RSJ International Conference on Intelligent Robots and Systems (IROS)*, 2024, pp. 1124–1129.
- [45] J. Li, S. Yuan, M. Cao, T.-M. Nguyen, K. Cao, and L. Xie, "Hcto: Optimality-aware lidar inertial odometry with hybrid continuous time optimization for compact wearable mapping system," *ISPRS Journal of Photogrammetry and Remote Sensing*, vol. 211, pp. 228–243, 2024.
- [46] T. H. Nguyen, S. Yuan, and L. Xie, "Vr-slam: A visual-range simultaneous localization and mapping system using monocular camera and ultra-wideband sensors," in *arXiv preprint arXiv:2303.10903*, 2023.
- [47] T.-M. Nguyen, D. Duberg, P. Jensfelt, S. Yuan, and L. Xie, "SlicT: Multi-input multi-scale surfel-based lidar-inertial continuous-time odometry and mapping," *IEEE Robotics and Automation Letters*, vol. 8, no. 4, pp. 2102–2109, 2023.
- [48] T. Jin, X. Xu, Y. Yang, S. Yuan, T.-M. Nguyen, J. Li, and L. Xie, "Robust loop closure by textual cues in challenging environments," *IEEE Robotics and Automation Letters*, vol. 10, no. 1, pp. 812–819, 2025.
- [49] S. Yuan and H. Wang, "Autonomous object level segmentation," in *Proceedings of International Conference on Control, Automation, Robotics and Vision (ICARCV 2014)*, 2014, pp. 33–37.
- [50] H. Wang, S. Yuan, and K. Wu, "Heterogeneous stereo: A human vision inspired method for general robotics sensing," in *TENCON 2017-2017 IEEE Region 10 Conference*. IEEE, 2017, pp. 793–798.
- [51] H. Cao, Y. Xu, J. Yang, P. Yin, X. Ji, S. Yuan, and L. Xie, "Reliable spatial-temporal voxels for multi-modal test-time adaptation," in *Computer Vision – ECCV 2024*, A. Leonardis, E. Ricci, S. Roth, O. Russakovsky, T. Sattler, and G. Varol, Eds. Springer Nature Switzerland, 2025, pp. 232–249.
- [52] T.-M. Nguyen, S. Yuan, T. H. Nguyen, P. Yin, H. Cao, L. Xie, M. Wozniak, P. Jensfelt, M. Thiel, J. Ziegenbein *et al.*, "Mcd: Diverse large-scale multi-campus dataset for robot perception," in *Proceedings of the IEEE/CVF Conference on Computer Vision and Pattern Recognition*, 2024, pp. 22304–22313.
- [53] H. Cao, Y. Xu, J. Yang, P. Yin, S. Yuan, and L. Xie, "Mopa: Multi-modal prior aided domain adaptation for 3d semantic segmentation," in *2024 IEEE International Conference on Robotics and Automation (ICRA)*. IEEE, 2024, pp. 9463–9470.
- [54] —, "Multi-modal continual test-time adaptation for 3d semantic segmentation," in *Proceedings of the IEEE/CVF International Conference on Computer Vision*, 2023, pp. 18809–18819.
- [55] Y. Yang, S. Yuan, and L. Xie, "Overcoming catastrophic forgetting for semantic segmentation via incremental learning," in *2022 17th International Conference on Control, Automation, Robotics and Vision (ICARCV)*. IEEE, 2022, pp. 299–304.
- [56] M. A. Esfahani, H. Wang, K. Wu, and S. Yuan, "Unsupervised scene categorization, path segmentation and landmark extraction while traveling path," in *2020 16th International Conference on Control, Automation, Robotics and Vision (ICARCV)*. IEEE, 2020, pp. 190–195.
- [57] M. Cao, T.-M. Nguyen, S. Yuan, A. Anastasiou, A. Zacharia, S. Papaioannou, P. Kolios, C. G. Panayiotou, M. M. Polycarpou, X. Xu *et al.*, "Cooperative aerial robot inspection challenge: A benchmark for heterogeneous multi-uav planning and lessons learned," *arXiv preprint arXiv:2501.06566*, 2025.
- [58] M. Cao, K. Cao, S. Yuan, K. Liu, Y. L. Wong, and L. Xie, "Path planning for multiple tethered robots using topological braids," in *Robotics: Science and Systems*, 2023.
- [59] M. Cao, K. Cao, S. Yuan, T.-M. Nguyen, and L. Xie, "Neptune: non-entangling trajectory planning for multiple tethered unmanned vehicles," *IEEE Transactions on Robotics*, vol. 39, no. 4, pp. 2786–2804, 2023.
- [60] Z. Liu, H. Mao, C.-Y. Wu, C. Feichtenhofer, T. Darrell, and S. Xie, "A convnet for the 2020s," *Proceedings of the IEEE/CVF Conference on Computer Vision and Pattern Recognition (CVPR)*, 2022.
- [61] A. Radford, J. W. Kim, C. Hallacy, A. Ramesh, G. Goh, S. Agarwal, G. Sastry, A. Askell, P. Mishkin, J. Clark *et al.*, "Learning transferable visual models from natural language supervision," in *International conference on machine learning*. PMLR, 2021, pp. 8748–8763.
- [62] D. Duberg and P. Jensfelt, "Ufomap: An efficient probabilistic 3d mapping framework that embraces the unknown," *IEEE Robotics and Automation Letters*, vol. 5, no. 4, pp. 6411–6418, 2020.
- [63] F. Afrati, S. Cosmadakis, C. H. Papadimitriou, G. Papageorgiou, and N. Papakostantinou, "The complexity of the travelling repairman problem," *RAIRO-Theoretical Informatics and Applications*, 1986.
- [64] Y. Zhao, L. Yan, H. Xie, J. Dai, and P. Wei, "Autonomous exploration method for fast unknown environment mapping by using uav equipped with limited fov sensor," *IEEE Transactions on Industrial Electronics*, pp. 1–10, 2023.
- [65] R. Tinós, K. Helsgaun, and D. Whitley, "Efficient recombination in the lin-kernighan-helsgaun traveling salesman heuristic," in *Parallel Problem Solving from Nature–PPSN XV: 15th International Conference, Coimbra, Portugal, September 8–12, 2018, Proceedings, Part 1 15*. Springer, 2018, pp. 95–107.
- [66] T. Cheng, L. Song, Y. Ge, W. Liu, X. Wang, and Y. Shan, "Yolo-world: Real-time open-vocabulary object detection," in *Proceedings of the IEEE/CVF Conference on Computer Vision and Pattern Recognition*, 2024, pp. 16901–16911.
- [67] X. Zhou, X. Wen, Z. Wang, Y. Gao, H. Li, Q. Wang, T. Yang, H. Lu, Y. Cao, C. Xu *et al.*, "Swarm of micro flying robots in the wild," *Science Robotics*, vol. 7, no. 66, p. eabm5954, 2022.
- [68] Z. Wang, X. Zhou, C. Xu, and F. Gao, "Geometrically constrained trajectory optimization for multicopters," *IEEE Transactions on Robotics*, vol. 38, no. 5, pp. 3259–3278, 2022.
- [69] P. Wu, Y. Mu, B. Wu, Y. Hou, J. Ma, S. Zhang, and C. Liu, "Voronav: Voronoi-based zero-shot object navigation with large language model," in *Proceedings of the 41st International Conference on Machine Learning (ICML)*, 2024.
- [70] S. K. Ramakrishnan, A. Gokaslan, E. Wijmans, O. Maksymets, A. Clegg, J. Turner, E. Undersander, W. Galuba, A. Westbury, A. X. Chang *et al.*, "Habitat-matterport 3d dataset (hm3d): 1000 large-scale 3d environments for embodied ai," *arXiv preprint arXiv:2109.08238*, 2021.
- [71] M. Labbé and F. Michaud, "Rtab-map as an open-source lidar and visual simultaneous localization and mapping library for large-scale and long-term online operation," *Journal of field robotics*, 2019.